

Modeling Ion Beam Neutralization and Near-Thruster Plume Interactions

IEPC-2005-270

Lubos Brieda* and Douglas VanGilder†

Air Force Research Laboratory, Edwards AFB, CA 93524

Joseph Wang‡

Virginia Polytechnic Institute and State University, Blacksburg, VA, 24061-0203

Ion thruster plume interaction has been studied extensively in recent years. While most existing plume models have focused on charge-exchange ion interactions with the spacecraft and/or plume-induced contamination, few studies have examined the detailed physics near the thruster exit. In particular, the ion beam neutralization process and the characteristics of the neutralizing electrons are not well understood. This paper presents a full-PIC model for the near-thruster plume of a single thruster. A multi-domain model, which splits the domain into a near-cathode region and a near-plume region, is used to obtain velocity distribution of the neutralizing electrons. This simulation is compared with one that assumes a pre-neutralized beam and another that uses a floating cathode potential.

I. Introduction

Numerical modeling has been used extensively to study the interaction of electric thruster plume with spacecraft. Most codes simplify the plasma dynamics by tracking only the heavy particles (ions and neutrals), while making assumptions about the distribution of the electrons. The mass of the electrons, and thus the difference in time scales of the various species, makes a full Particle-In-Cell (PIC)¹ algorithm computationally challenging. A common approach is to assume that the electron distribution follows the Boltzmann relationship, based on user supplied values of reference parameters. A typical hybrid-PIC algorithm thus cannot correctly resolve the physics in the near-thruster region, which is dominated by a non-neutral plasma and an interaction of neutralizing electrons with the beam. No simulation models are currently available to investigate the near-thruster plume, and the ion beam neutralization process is still not well understood.

Understanding of the neutralization process will become even more important for electric thruster clusters that are being considered for future space applications. Such a cluster system may use a single cathode to neutralize ion beams emitted from multiple thrusters. Already, several cluster configurations were tested experimentally by Beal and Hargus.^{2,3} However, experimental measurements can provide only a limited amount of information on the motion of the electrons. The effectiveness of beam neutralization by a shared neutralizer is still not clear, and there is no generally accepted optimal configuration for electric thruster clusters.

This paper presents results from numerical modeling of neutralization of a single ion thruster. An attempt has been made to improve results obtained in a previous work.⁴ Primarily, the effect of the simplified cathode model on electron dynamics is investigated. In the present study, a multi-domain formulation was used to obtain initial distribution of electrons near the cathode. The electrons were then sampled from the distribution list and then introduced into the ion beam domain. This approach was necessary, because the

*Research Scientist, ERC Inc., lubos.brieda@edwards.af.mil

†Aerospace Engineer, AFRL/PRSS, douglas.vangilder@edwards.af.mil

‡Associate Professor, Department of Aerospace and Ocean Engineering, jowang@vt.edu

Report Documentation Page

Form Approved
OMB No. 0704-0188

Public reporting burden for the collection of information is estimated to average 1 hour per response, including the time for reviewing instructions, searching existing data sources, gathering and maintaining the data needed, and completing and reviewing the collection of information. Send comments regarding this burden estimate or any other aspect of this collection of information, including suggestions for reducing this burden, to Washington Headquarters Services, Directorate for Information Operations and Reports, 1215 Jefferson Davis Highway, Suite 1204, Arlington VA 22202-4302. Respondents should be aware that notwithstanding any other provision of law, no person shall be subject to a penalty for failing to comply with a collection of information if it does not display a currently valid OMB control number.

1. REPORT DATE 31 AUG 2005	2. REPORT TYPE Conference Paper	3. DATES COVERED 00-08-2005 to 00-08-2005	
4. TITLE AND SUBTITLE Modeling Ion Beam Neutralization and Near-Thruster Plume Interactions - PREPRINT		5a. CONTRACT NUMBER	
		5b. GRANT NUMBER	
		5c. PROGRAM ELEMENT NUMBER	
6. AUTHOR(S) Lubos Brieda; Douglas VanGilder		5d. PROJECT NUMBER 4847	
		5e. TASK NUMBER 0052	
		5f. WORK UNIT NUMBER	
7. PERFORMING ORGANIZATION NAME(S) AND ADDRESS(ES) Air Force Research Laboratory (AFMC), AFRL/PRSS, 1 Ara Road, Edwards AFB, CA, 93524-7013		8. PERFORMING ORGANIZATION REPORT NUMBER AFRL-PR-ED-TP-2005-319	
9. SPONSORING/MONITORING AGENCY NAME(S) AND ADDRESS(ES) Air Force Research Laboratory (AFMC), AFRL/PRS, 5 Pollux Drive, Edwards AFB, CA, 93524-7048		10. SPONSOR/MONITOR'S ACRONYM(S) XC	
		11. SPONSOR/MONITOR'S REPORT NUMBER(S) AFRL-PR-ED-TP-2005-319	
12. DISTRIBUTION/AVAILABILITY STATEMENT Approved for public release; distribution unlimited			
13. SUPPLEMENTARY NOTES Presented at the 29th International Electric Propulsion Conference, Princeton, NJ, 31 Oct - 4 Nov 2005.			
14. ABSTRACT Ion thruster plume interactions has been studied extensively in recent years. While ost existing plume models have focused on charge-exchange ion interactions with the spacecraft and/or plume-induced contamination, few studies have examined the detailed physics near the thruster exit. In particular, the ion beam neutralization process and the characteristics of the neutralizing electrons are not well understood. This paper presents a full-PIC model for the near-thruster plume of a single thruster. A multi-domain model, which splits the domain into a near-cathode region and a near-plume region, is used to obtain velocity distribution of the neutralizing electrons. This simulation is compared with one that assumes a pre-neutralized beam and another that uses a floating cathode potential.			
15. SUBJECT TERMS			
16. SECURITY CLASSIFICATION OF:			17. LIMITATION OF ABSTRACT
a. REPORT unclassified	b. ABSTRACT unclassified	c. THIS PAGE unclassified	
			18. NUMBER OF PAGES 12
			19a. NAME OF RESPONSIBLE PERSON

main simulation mesh was not fine enough to resolve the plasma parameters in the high-density region near the cathode tip.

II. DRACO ES-PIC Code

A 3D plasma simulation code, called DRACO, was used in this work. DRACO was developed within the AFRL COLISEUM framework, which is a collection of modules capable of modeling the dynamics of electric thruster plumes and their interactions with spacecraft surfaces.⁵

The DRACO module tracks particles on a Cartesian mesh, which has been overlaid with a secondary tetrahedral mesh.⁶ This secondary mesh allows DRACO to resolve surface geometries with detail beyond the standard "stair-case" representation attainable on Cartesian grids. Surface definition is specified using planar cuts of *interface* tetrahedrons.

The main COLISEUM package contains support for loading of triangular meshes from input files using standard formats such as Ansys or Abaqus. The interface mesh is generated automatically by DRACO's helper module called VOLCAR. The actual intersection process is described in a greater detail in Ref.7.

The interface cuts are used to perform particle surface interactions, and, depending on the chosen solver, to obtain the plasma potential, ϕ . The plasma potential is computed from the Poisson's equation,

$$\nabla^2 \phi = -\frac{\rho}{\varepsilon_0} \quad (1)$$

using the DADI⁸ scheme. In the above equation, ρ is the charge density of the particles, C/m³, and ε_0 is the permittivity of free space, 8.854×10^{-12} F/m. The charge density is computed from the individual contributions of the ions and the electrons, $\rho = q(n_i - n_e)$, where $n_{i,e}$ is the number density of the ions or electrons. In the Particle-In-Cell (PIC) method, the number density is obtained by coupling the particles with the grid through particle *shape factors*,

$$n_k = \sum_i w_i S(x_i - x_k) \quad (2)$$

where x_k is the position of a grid node, and w_i is the specific weight of the macroparticle. In this work, the shape and size of the particles was identical to the Cartesian cell. This first-order representation reduces the simulation noise associated with the zeroth-order (point particle) model, while still allowing a simple particle-mesh weighing algorithm. The electric field, \vec{E} , is then computed from

$$\nabla \phi = -\vec{E} \quad (3)$$

using the standard centered finite-difference method. Particle velocity is adjusted according to the Lorentz force,

$$m \frac{\partial \vec{v}}{\partial t} = \vec{F} = q \left(\vec{E} + \vec{v} \times \vec{B} \right) \quad (4)$$

where m = particle mass, kg
 \vec{v} = particle velocity, m/s
 q = particle charge, C
 \vec{E} = electric field, V/m
 \vec{B} = magnetic field, T

The electro-static (ES) formulation, implemented by DRACO, assumes that $\partial \vec{B} / \partial t = 0$. No static background field was used in the current simulation, and hence the force acting on the particles was simply

$$m \frac{\partial \vec{v}}{\partial t} = \vec{F} = q \vec{E} \quad (5)$$

The equation of motion for the particles is

$$\frac{\partial \vec{x}}{\partial t} = \vec{v} \quad (6)$$

This equation is integrated numerically along with eq. 5 using the *leapfrog* method with a finite timestep Δt . Final position of the particles is checked for surface interactions. Particles leaving the simulation domain are

either removed from the simulation, or are reintroduced according to prescribed boundary conditions. New particles are introduced by sampling particle sources. This process repeats until a user specified condition, such as reaching a steady-state, or exceeding a maximum number of timesteps, is satisfied.

III. Neutralization Modeling

A. Thruster Model

The ion thruster used in this study is based on the 40cm NASA Evolutionary Xenon Thruster (NEXT). Surface definition of the thruster is shown in figure 1. This mesh was generated with MSC.Patran. It should be noted that a dimensional drawing of the thruster was not available to the authors, and hence the thruster geometry was generated by collecting data from several relevant sources.^{9,10}

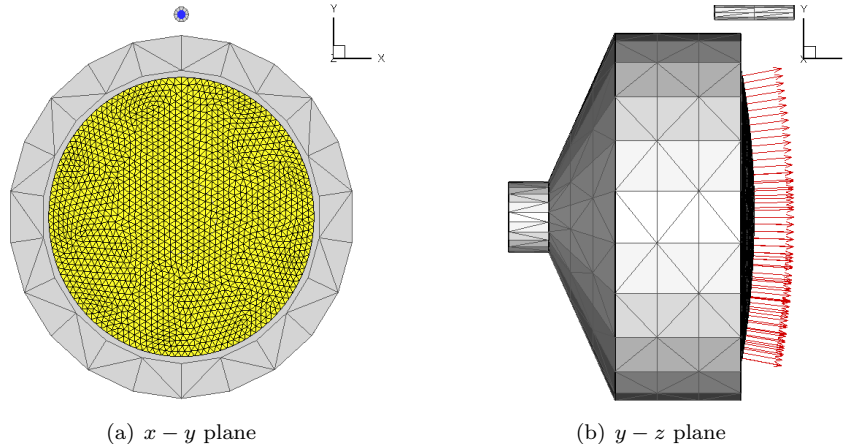


Figure 1. Surface mesh of the ion thruster. Yellow region indicates source triangles emitting ions. Electrons are injected from the small blue region at the tip of the cathode. The physical curvature of the ion optics was used to introduce curvature to the ion beam. The normal vectors of source elements, shown by red arrows, roughly indicate the initial divergence of the beam.

COLISEUM provides a general support for surface sources. Various particle production models can be associated with a collection of surface triangles. Generally, the particles are introduced with a mean velocity in the direction of the surface normal vector. Physical curvature of the surface will result in a divergence of the ion beam. This feature was used in the present work, as can be seen in figure 1(b), which shows the normal vectors of the surface elements. Curvature of the surface mesh resulted in approximately a 15° beam divergence. Beam flatness (ratio of current density between the centerline and the edge) was adjusted by biasing the mass production rate of the source elements, according to current density measurements of Soulas.¹¹ The thruster operating condition was set to 1.2A of beam current, with ions injected with an average velocity of 34,400m/s (corresponding to 3510s ISP) and a temperature of 0.1eV.¹²

Several assumptions were made about the plume dynamics. First, collisions were ignored. The mean free path, λ_m , for an electron-ion collision can be estimated from Ref.¹³

$$\lambda_m = \frac{1}{n\sigma} = \frac{16\pi\epsilon_0^2 m^2 v^4}{ne^4} \quad (7)$$

For plasma density, $n \sim 10^{15} \text{ m}^{-3}$ and electron velocities, $v \sim 10^6 \text{ m/s}$, λ_m is $O(1)\text{m}$. This length is similar to the characteristic dimension of the domain. Coulomb collisions thus do not play a significant role. Neutral-neutral and neutral-ion collisions are expected to be more frequent, leading to a particle scatter and creation of charge-exchange ions. While the effect of these collisions is significant in the study of interaction of the plume with the spacecraft, this work concentrated on the dynamics of the electrons and their interaction with the beam ions.

Second, the plume was assumed to consist only of singly-charged ions and electrons. While the neutral density near the thruster exit can exceed the ion density, the neutrals interact with ions exclusively through collisions. In the absence of collisions, tracking of neutrals would only slow down the simulation. Doubly-

charged ions were not included since their actual distribution was not known. Furthermore, production of doubly-charged ions is not desired because it leads to faster thruster erosion.

Finally, the thruster was assumed to be a perfect conductor. Any absorbed electrons were re-injected from their original source at the next timestep. Collection of an electron current in a space environment would lead to a decrease in the thruster potential, thus preventing an excessive build-up of negative charge. However, the current version of DRACO does not contain functionality to model this behavior.

B. Dimensional Scaling and Boundary Conditions

Interaction of the electrons with the ions, and their containment in the beam was examined by modeling a pre-neutralized beam. This beam pre-neutralization was accomplished by injecting both ions and electrons from the optics. Due to symmetry, only a quarter domain was simulated. The domain is shown in figure 2(a). The cell size was set to $2 \times 10^{-4} \sim \lambda_D$, and the simulation contained $50 \times 50 \times 90$ cells.

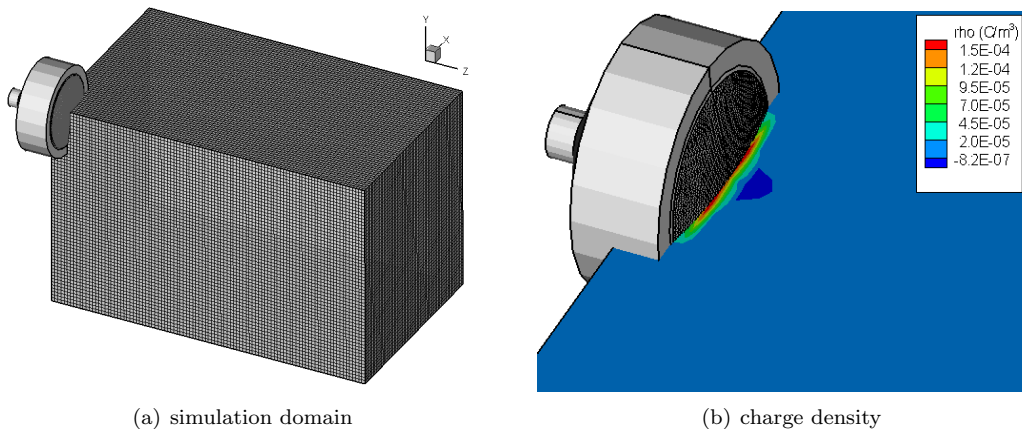


Figure 2. Simulation domain used to study electron dynamics in a pre-neutralized beam. Right plot (b) shows charge density at steady-state if a uniform cell size of 2cm was used. Large cell size leads to formation of a virtual anode.

The simulation was performed on a thruster *scaled-down* by a factor of 100:1. Plasma density at the thruster exit was retained by decreasing the emission current by 10,000 (100×100). This scaling was necessary, since resolving the Debye length on the full-sized domain would require a numerically excessive number of computational nodes (over 1 billion). Total number of nodes could be reduced by increasing the simulation cell size to about $100\lambda_D$. However, as figure 2(b) shows, doing so results in a development of a virtual anode¹⁴ at the thruster exit, despite the thruster injecting equal electron and ion currents. The virtual anode develops since the PIC formulation replaces point sized particles with particles the size of the cell. No detail is available at length scales smaller than the cell size. Furthermore, λ_D specifies the smallest distance at which quasi-neutrality can be assumed. Motion of the electrons is influenced by electric fields which arise due to local charge non-neutralities. A simulation cell which is several orders of magnitude larger than the Debye length is not capable of resolving these charge variations, thus proper mixing of electrons with the ions is not achieved.

The Neumann ($\partial\phi/\partial\hat{n} = 0$) boundary condition was specified for the potential solver on all external faces. A reflective boundary condition was applied for particles along the planes of symmetry. Particle motion through the remaining domain boundaries was controlled by an *energy* boundary condition. As was described in a greater detail in Ref. [4], conservation of energy dictates that, in absence of other potential drops and energy sources, a particle traveling from rest through a potential hump must reach a velocity inflection point. Since kinetic energy must remain non-negative, the particle motion will reflect, and the particle will be trapped in a potential hill. Due to a limited domain span, the inflection point may be located outside of the domain boundary. This case then leads to a removal of electrons which should have been retained by the simulation. The energy boundary attempts to retain these electrons by reflecting any particles with kinetic energy insufficient to escape the potential drop. The required potential energy is calculated from the difference between the beam core potential and ϕ_∞ .

C. Cathode Model

Jameson, et. al.¹⁵ measured approximately 5V of potential drop through the cathode, leading to electron exit velocities of approximately 10^6 m/s. A cathode with a keeper exit diameter of 1.2cm was used in this work. From $j = nev$, the electron density at the cathode exit is $\sim 6 \times 10^{16}$ m/s. Electron temperature at the exit is ~ 1 eV, yielding $\lambda_D \sim 3 \times 10^{-5}$ m/s, or about $1/10^{th}$ of the cell size. Injection of electrons from the cathode without resolving the Debye length at the cathode tip resulted in development of a virtual cathode.⁷ The only electrons that were able to escape were those born with a strong radial velocity component.

In this work, two cathode models are examined. The first model uses a floating cathode with a limiting value for charge density near the keeper exit. This formulation is identical to work done in Ref. [4]. By floating the potential, the strong axial potential gradient is eliminated, and the electrons can leave the cathode. Charge density around the cathode was limited to prevent development of strong self-induced fields. The electrons were also injected with small velocities, so they could immediately start following the electric field.

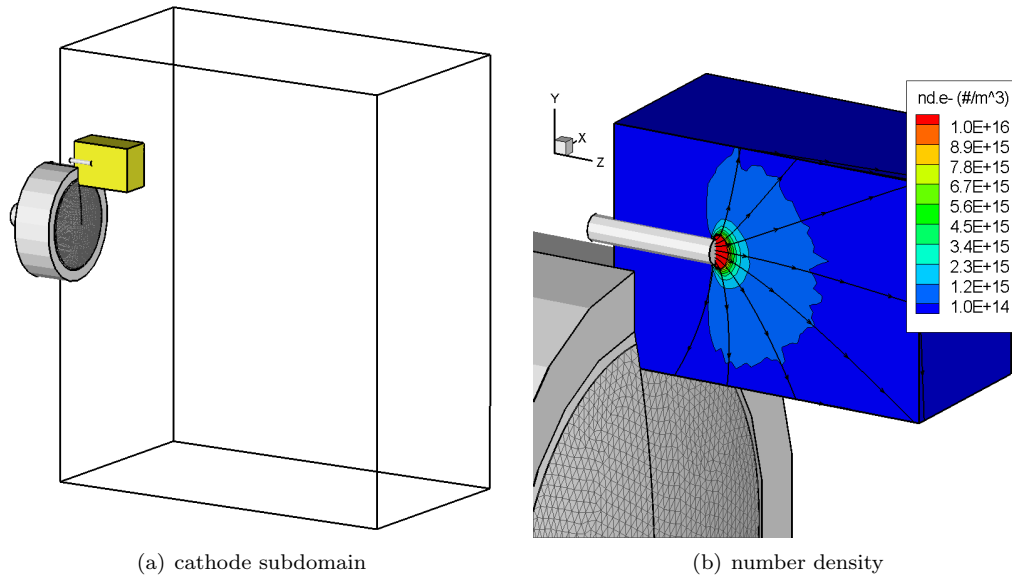


Figure 3. The yellow shaded region indicates the subdomain used in cathode modeling. Boundary of the mesh used in neutralization modeling and the thruster are shown for scale. Electrons were sampled from the entire subdomain in subsequent neutralization modeling. Right plot (b) shows the electron density and velocity stream lines at steady state.

While this approach resulted in a free extraction of electrons, it also contributed to a non-physical plume potential profile and electron temperature. In this work, a multi-domain cathode model was used to obtain initial distribution of the neutralizing electrons. A secondary simulation was performed on a sub-domain region surrounding the cathode. Cell size was decreased to 5×10^{-5} m, and the mesh consisted of $30 \times 40 \times 60$ nodes. Potential drop of 10V was applied between the cathode, and the anode, which was represented by the body of the ion thruster. The subdomain is shown in figure 3(a). Boundary of the primary mesh is included for scale.

Figure 3(b) shows the number density of the electrons in the sub-domain after reaching a steady-state. Streamlines of electron velocities are also shown. The electrons are seen to expand uniformly. Geometry of the simulation results in a strong axial electric field along the cathode centerline. Electrons born in this region are accelerated out of the domain. The remaining electrons are slowed down by the potential gradient, and are attracted back to the anode. The velocity distribution at steady-state is shown in figure 4. The electrons retain their initial injection Maxwellian distribution.

This sub-domain acted as a volumetric source during the main neutralization modeling. Positions and velocities of 100,000 randomly chosen electrons were sampled to a data file. A new particle source has been written to return a randomly chosen entry from the list. The potential drop between the cathode and the anode was fixed at 10V.

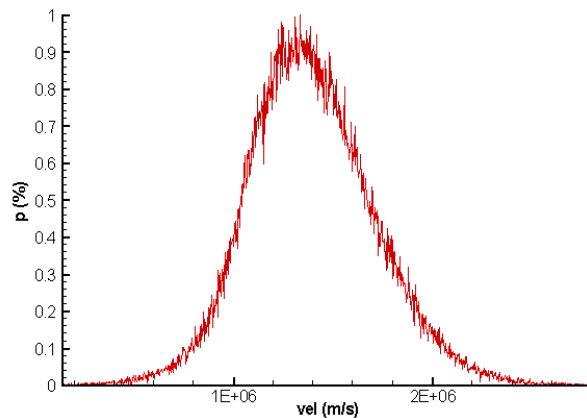


Figure 4. Velocity distribution of the electrons in the cathode subdomain.

IV. Results

A. Reference Case

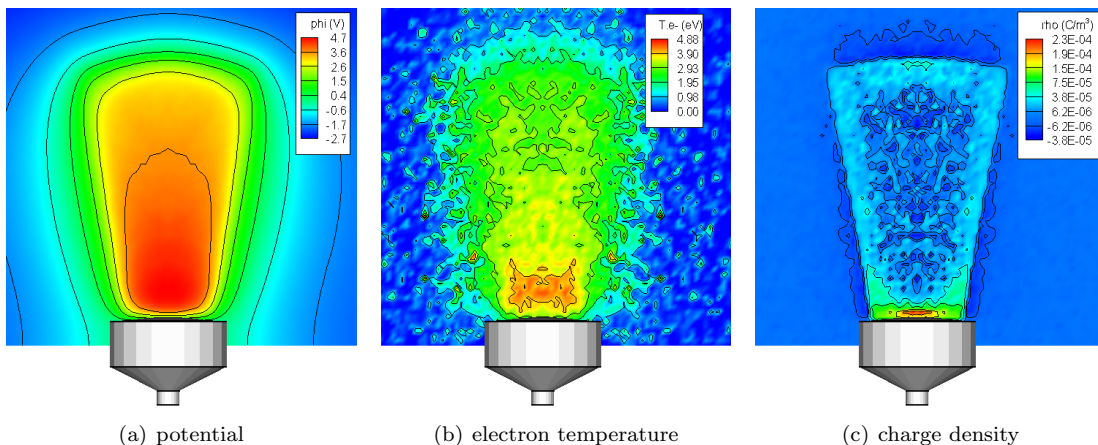


Figure 5. Potential, electron temperature, and charge density after 3×10^{-7} seconds, for a single thruster.

Plots in figure 5 show the plasma parameters on the plane of symmetry obtained using the pre-neutralized reference configuration (RF). A distinct beam profile is seen in the plot of the potential. Potential reaches about 4.7V in the core near the thruster exit, and is seen to decrease with beam divergence. This value closely agrees with experimental measurements.¹⁶ Electron temperature, computed by assuming Maxwellian distribution, reaches a similar value, and is also seen to decrease uniformly with density. Figure 5(c) shows the charge density, $\rho = q(n_i - n_e)$. A good neutrality ratio is indicated by light-blue shading. The charge density in the beam is seen to be slightly positive, which leads to the positive potential in the beam. An electron sheath is seen to surround the beam. This sheath is responsible for the containment of the electrons.

The electric field components, $\vec{E} = -\nabla\phi$, are shown in figures 6(a) and 6(b). Both the radial and the axial components are approximately zero in the bulk of the beam. Hence, the acceleration of the electrons is expected to be limited to the regions near the edge of the beam, with electrons moving at constant velocities inside the beam core. The motion of the electrons is highly random (fig. 6(c)), even though they were originally injected in the axial direction, using a Maxwellian source with $T_e = 1\text{eV}$. Due to their high mobility, the electrons seem to have only a weak memory of their injection distributions.

Maxwellian temperature obtained from the simulation is compared to the polytropic relationship

$$T = T_0 \left(\frac{n}{n_0} \right)^{(\gamma-1)} \quad (8)$$

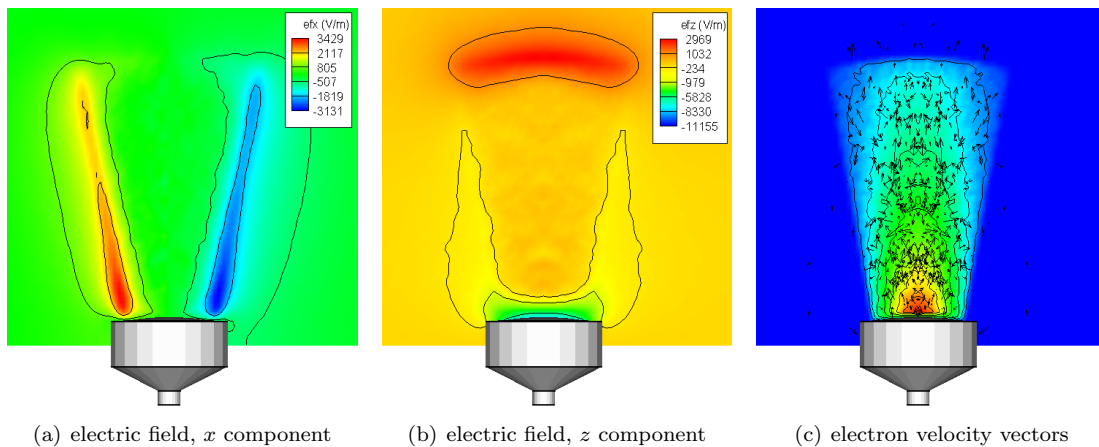


Figure 6. Electric field and electron velocity vectors for the reference case. Electrons were injected from the optics using Maxwellian distribution with $T_e = 1\text{eV}$.

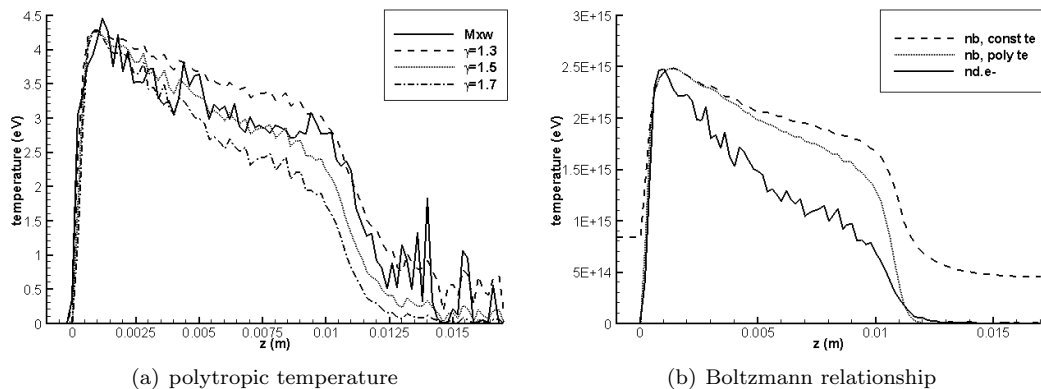


Figure 7. Comparison of numerical temperature to the polytropic model, and comparison of simulation electron density to prediction using Boltzmann model.

for three values of γ in figure 7(a). Reference temperature and density were chosen to correspond to the values in the beam core, 4.2eV and $2.5 \times 10^{15} \text{ m}^{-3}$, respectively. Neither of the three chosen gamma values was able to produce an exact match, however, the temperature seems to roughly follow the polytropic relationship with $\gamma \sim 1.4$.

Numerical electron density was also compared against the Boltzmann relationship, which states that a direct relationship exists between plasma potential and plasma density,

$$n_e = n_0 \exp\left(\frac{\phi - \phi_0}{kT_0}\right) \quad (9)$$

Again, plasma properties in the beam core were used for the reference values. Reference potential was set to 4.7V. The relationship was computed using both constant reference temperature (4.2eV), and polytropic temperature with $\gamma = 1.4$. Generally, the agreement is not very good, as figure 7(b) shows. Best agreement is achieved near the core, which is expected, since this location corresponds to the point at which the reference values were sampled. The simulation electron density drops off faster than predicted by the model. The disagreement is reduced by using the polytropic temperature, however, a significant discrepancy still remains. A better agreement could be achieved by adjusting the reference parameters; this approach however requires prior knowledge of the solution.

B. Single Thruster

1. Floating Cathode

The simulation domain used in single thruster neutralization modeling can be seen in figure 3(a). Due to symmetry, only a half domain was simulated. Reflective particle boundary condition was used along the symmetric face. The grid dimensions were $50 \times 100 \times 90$, and the mesh used a uniform cell spacing of $2 \times 10^{-4} \text{ m}$.

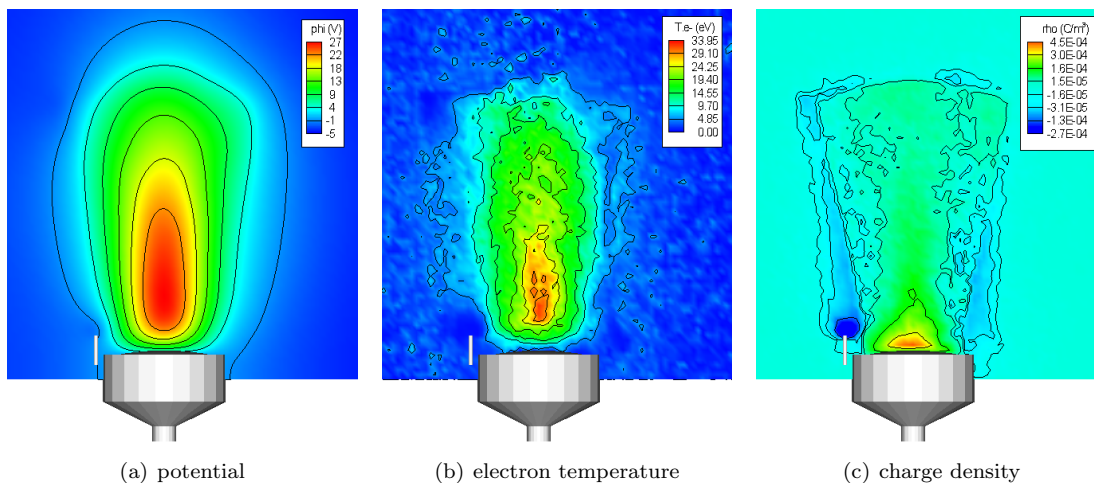


Figure 8. Potential, electron temperature, and charge density after 3×10^{-7} seconds, for a single thruster.

Figure strip 8 shows potential, temperature and charge density obtained by floating the potential on the cathode. Results for this configuration (NSF) were expected to agree with the reference case RF, but a quick comparison with figure 8 indicates a high degree of divergence. The beam shape is no longer well resolved. Furthermore, the beam potential has increased to 27V and the maximum electron temperature has increased to 34eV.

The high values of beam potential and temperature point to a non-neutral beam. However, over-saturation of the beam with electrons by increasing the cathode current led to turning of the beam towards the cathode, but the potential drop across the beam did not change significantly. The beam temperature also remained high.

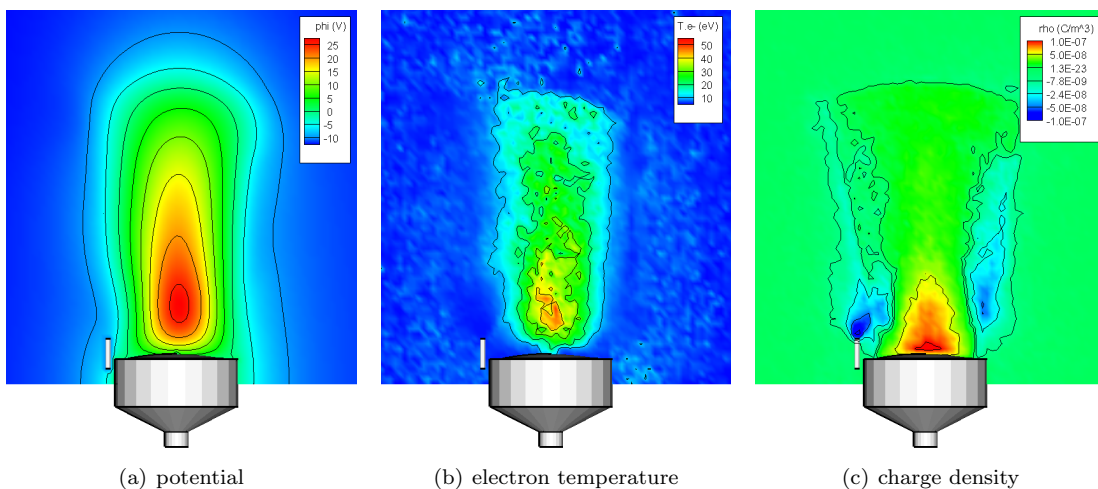


Figure 9. Potential, electron temperature, and charge density after 3×10^{-7} seconds, for a single thruster.

2. Multi-domain Cathode model

Therefore, lack of electrons did not seem to be the main factor contributing to the non-physical results. In this work, the influence of the cathode model on the results was investigated by replacing the floating potential model with the multi-domain formulation. Figure 9 shows plasma properties obtained with the new model. Important to note is the region near the cathode. The charge density plot shows a clear turning of the electron plume towards the beam. This behavior was not achieved in the floating cathode case. The electron sheath surrounding the beam is also better resolved, and the overall range of ρ has decreased which indicates a better neutrality ratio. However, no significant improvement in results is seen. Although the beam potential has decreased slightly to about 25V, the core temperature remains high and non-polytropic.

C. Analysis

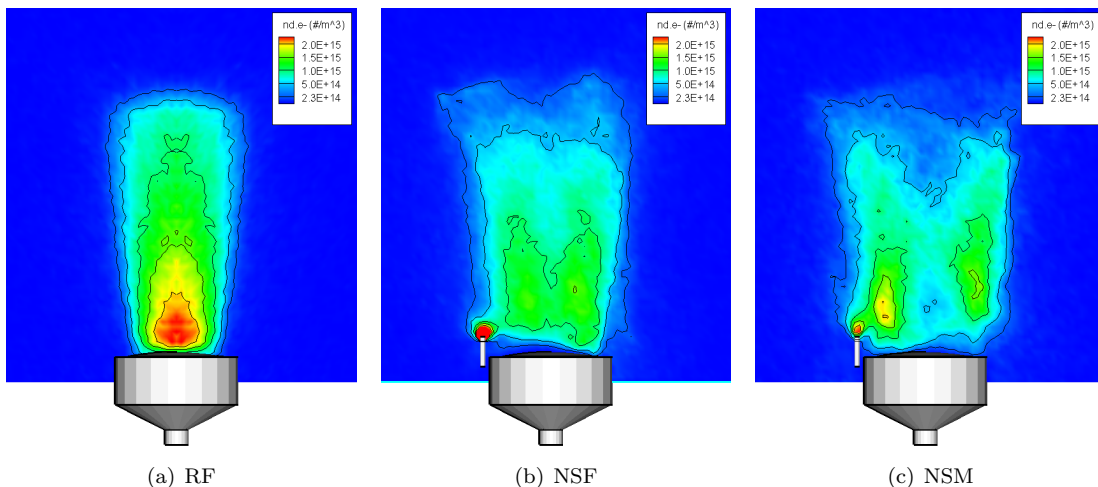


Figure 10. Electron density contour for the three cases. A clear distinction is seen between the reference case and the two cases in which electrons were injected from the cathode.

The new cathode model failed to resolve the fundamental problem leading to the non-physical results. Figure 10 shows the electron densities for the three cases. A clear difference is seen between the reference case, and the two cathode cases. The electron density in the reference case follows the Boltzmann relationship, with highest density coinciding with the beam core. The electrons instead seem to concentrate along the edges of the beam in the two cathode runs.

Existence of an almost uniform high-temperature region along beam axis in both NS cases indicates mixing of electron streams with opposing directions. Thus, the collective dynamics of the electrons seem to be driven by oscillations around the beam core. In other words, using a 1-D approximation, electrons injected at the cathode fall into the potential well created by the beam. The velocity of the electrons increases until they pass the beam centerline. The velocity then begins to decrease as they travel up the well. The electrons come to a stop at a point where all kinetic energy has been exhausted. Assuming initial injection at 0m/s, the potential drop on both sides of the well will be equal. The increased electron densities seen along the beam edge in cases NSF and NSM are a direct consequence of electrons coming to a stop and turning around.

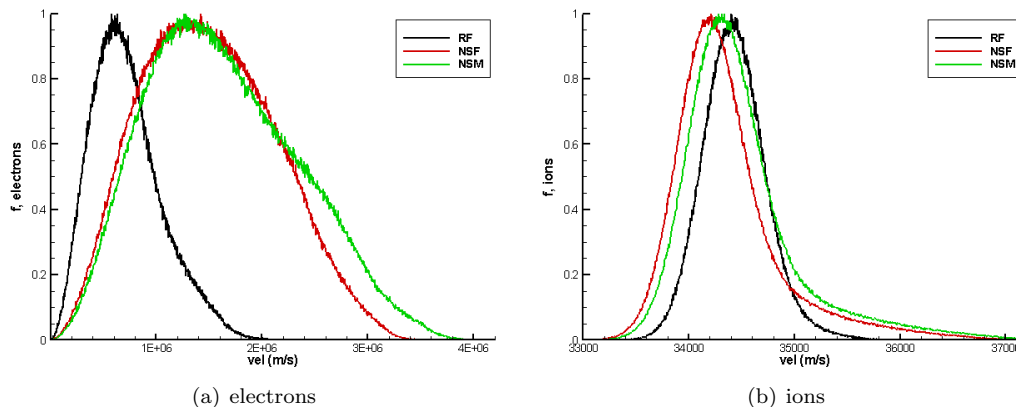


Figure 11. Electron and ion velocity distribution at the end of simulation.

The potential in the beam adjusts as a direct response to the oscillations of the electrons. Retention of the electrons in the beam requires that the $PE_{beam} \geq KE_{e,max}$. Using $PE = KE$ and total potential drops between the cathode and the beam of 4.7V and 25V, the mean velocity of the electrons oscillating around the beam core is expected to be 1.3×10^6 and 2.9×10^6 m/s for cases RF and NSx, respectively. This is confirmed by the tail of electron velocity histograms shown in figure 11(a). The red line (NSF) shows the distribution for the original floating cathode model. Comparison with the reference curve shows an increase in mean velocity. Even more important is the widening of the curve, which is indicative of a temperature increase. The shape of the curve remains close to Maxwellian. The green line indicates the electron velocity obtained with the new model. A small increase in number of fast moving particles is seen, but overall, the distribution remains comparable to NSF. A greater difference is seen in the ion velocities. Decrease in the size of the high potential region in the NSM case results in fewer electrons being slowed down by the strong potential gradient. The mean beam velocity for case NSM is closer to the reference configuration.

In order to obtain the Boltzmann relationship, the amplitude of the electron oscillations must decrease with time. This is analogous to the classical example of stability, in which a ball has been placed into a spherical cup. Displacement of the ball from the rest position at the bottom will result in simple oscillations about the bottom of the cup. In the absence of dissipative forces, the amplitude of oscillations will not change with time. However, in a realistic configuration, dissipation of energy due to non-conservative forces will result in a gradual decrease of the amplitude. After some time, the ball will come back to rest.

The simulation presented here does not contain any such dissipative force. Instead, the electrons keep oscillating around the potential drop of the beam. Hence, the electron density is not able to reach a Boltzmann-like relationship. Electrons in the reference case are not strongly influenced by this simplification, since they are born at the *bottom* of the potential well. Furthermore, their initial velocity is coincident with the direction of the beam ions. However, the electrons born at the cathode originate at the *top* of the potential well and flow into the beam radially.

Exchange of kinetic energy with massive particles would result in a large decrease in electron velocities, while only slightly influencing the motion of the ions. However, as was mentioned previously, collisions were ignored in this case, due to large mean-free paths, and hence low collision frequencies. More probable is the transfer of kinetic energy from the electrons to plasma waves. Figure 12 shows the total field energy versus simulation time. Clear oscillations develop after $t = 1.5 \times 10^{-7}$ seconds. The meaning of these oscillations is still not clear, however a decay is seen around $t = 2.4 \times 10^{-7}$. It is possible that the numerical setup of the problem is preventing development or growth of energy dissipating waves.

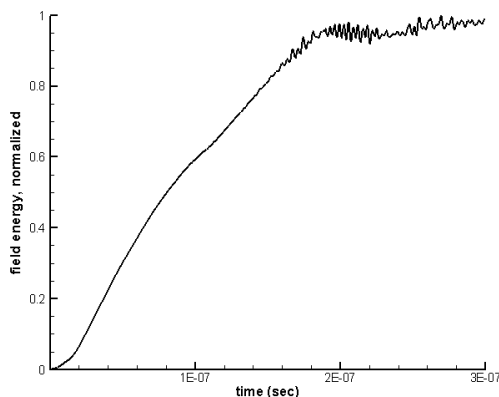


Figure 12. Total simulation field energy versus simulation time. A high-frequency wave is seen to develop after $t = 1.5 \times 10^{-7}$ seconds.

V. Conclusion

A new simulation model to study ion beam neutralization is being developed. This model uses a fully-kinetic formulation in which both electrons and ions are tracked as macro-particles. This formulation avoids problems associated with fluid modeling of the electrons, but introduces numerical difficulties. Most important is the necessity to resolve the local Debye length, otherwise the electrons fail to mix with the ions. Computationally excessive number of nodes would be required to resolve the Debye length on a full-scale geometry. Instead, a dimensional scaling approach was used, with thruster current adjusted such that plasma density at the thruster exit remained unchanged. This approach allowed for examining the neutralization process. Outflux of electrons at boundaries was prevented by reflecting all electrons with kinetic energies insufficient to escape the potential drop of the beam.

This simulation approach was used to model neutralization of the NASA NEXT ions thruster. A reference case was setup by injecting both electrons and ions from the optics. The potential solution showed a clear beam profile, with maximum potential of 4.7V. The electron temperature reached about 5eV in the core, and decreased polytropically with density. These results agree well with experimental data. The electron density was also compared to the Boltzmann model, but the two curves diverged for the chosen coefficients.

Simulation of a single thruster neutralized by an external cathode was also studied. The potential around the cathode could not be resolved correctly using the primary mesh, due to the cathode's small size and a high electron density near the tip. Instead, two approaches were investigated. In the first model, the cathode potential was allowed to float and charge density at the tip was fixed. The second model used a multi-domain formulation. Simulation of the near cathode region was performed first using a fine mesh, followed by sampling of random electrons to a data file. This distribution list was then used by primary simulation to introduce electrons from the volume described by the fine mesh.

Plasma properties in either cathode run did not agree with the reference case. Beam potential increased to about 25V and the temperature distribution no longer followed the polytropic relationship. Closer inspection of simulation results indicates that the electrons oscillate around beam. The amplitude of oscillations should decrease with time, however, this does not seem to be the case in the current simulation. Investigation into the primary mechanism and the actual modeling of the kinetic energy sink remain as future work.

References

- ¹Birdsall, C., and Langdon, A., *Plasma Physics Via Computer Simulations*, Institute of Physics Publishing, Philadelphia, 2000
- ²Beal, B., Gallimore, A., Haas, J., and Hargus, W., "Plasma Properties in the Plume of a Hall Thruster Cluster," *Journal of Propulsion and Power*, Vol. 20, No. 6, 2004
- ³Hargus, W., Cappelli, M., "Interactions Within a Cluster of Low Power Hall Thrusters," *AIAA/ASME/SAE/ASEE Joint Propulsion Conference and Exhibit*, 39th, Huntsville, AL, July 20-23, 2003.
- ⁴Brieda, L., Wang, J., "Modeling of Ion Thruster Beam Neutralization Using a Fully Kinetic ES-PIC Code," *AIAA/ASME/SAE/ASEE Joint Propulsion Conference and Exhibit*, 41th, Tucson, AZ, July 10-13, 2005

- ⁵Gibbons, M., Kirtley, D., VanGilder, D., and Fife, J., "Flexible Three-Dimensional Modeling of Electric Thrusters in Vacuum Chambers," AIAA-2003-4872, 2003
- ⁶Brieda, L., Pierru, J., Kafafy, R., and Wang, J., "Development of the DRACO Code for Modeling Electric Propulsion Plume Interactions," *AIAA/ASME/SAE/ASEE Joint Propulsion Conference and Exhibit*, 40th, Fort Lauderdale, FL, July 11-14, 2004
- ⁷Brieda, L., "Development of the DRACO ES-PIC Code and Fully-Kinetic Simulation of Ion Beam Neutralization", Master's Thesis, Aerospace and Ocean Eng. Dept., Virginia Tech, Blacksburg, VA, 2005
- ⁸Hewett, D., Larson, W., and Doss, S., "Solution of Simultaneous Partial Differential Equations Using Dynamic ADI: Solution of the Streamline Darwin Field Equations," *Journal of Computational Physics*, Vol. 101, 1992, pp. 11-24
- ⁹Patterson, M., et. al, "NEXT: NASA's Evolutionary Xenon Thruster," *AIAA/ASME/SAE/ASEE Joint Propulsion Conference and Exhibit*, 38th, Indianapolis, IN, July 7-10, 2002
- ¹⁰Soulas, G., Domonkos, M., and Patterson, M., "Performance evaluation of the NEXT ion engine," *AIAA/ASME/SAE/ASEE Joint Propulsion Conference and Exhibit*, 39th, Huntsville, AL, July 20-23, 2003
- ¹¹Soulas, G., Haag, T., and Patterson, M., "Performance evaluation of 40 cm ion optics for the NEXT ion engine," AIAA Paper 2002-3834, July 2002
- ¹²NASA Glenn Website, *NASA's Evolutionary Xenon Thruster (NEXT)*, <http://space-power.grc.nasa.gov/ppo/projects/next/accomp.html>
- ¹³Chen, F. F., *Introduction to Plasma Physics and Controlled Fusion, Volume 1*, Plenum Press, New York, 1984
- ¹⁴Wang, J., and Lai, S., "Virtual Anode in Ion Beam Emission in Space: Numerical Simulations," *Journal of Spacecraft and Rockets*, Vol. 34, No. 6, 1997
- ¹⁵Jameson, K., Goebel, D., and Watkins, R., "Hollow Cathode and Keeper-Region Plasma Measurements," *AIAA/ASME/SAE/ASEE Joint Propulsion Conference and Exhibit*, 41th, Tucson, AZ, July 10-13, 2005
- ¹⁶Kamhawi, H., Soulas, G., Patterson, M., and Frandina, M., "NEXT Ion Engine 2000 Hour Wear Test Plume and Erosion Results," *AIAA/ASME/SAE/ASEE Joint Propulsion Conference and Exhibit*, 40th, Fort Lauderdale, FL, July 11-14, 2004